




Article

The Effect of Variable Magnetic Field on Viscous Fluid between 3-D Rotatory Vertical Squeezing Plates: A Computational Investigation

Muhammad Kamran Alam ^{1,*}, Khadija Bibi ¹, Aamir Khan ¹ , Unai Fernandez-Gamiz ²  and Samad Noeiaghdam ^{3,4} 

¹ Department of Mathematics & Statistics, The University of Haripur, Haripur 22620, Pakistan; p109954@nu.edu.pk (K.B.); aamir.khan@uoh.edu.pk (A.K.)

² Nuclear Engineering and Fluid Mechanics Department, University of the Basque Country UPV/EHU, Nieves Cano 12, 01006 Vitoria-Gasteiz, Spain; unai.fernandez@ehu.eus

³ Industrial Mathematics Laboratory, Baikal School of BRICS, Irkutsk National Research Technical University, 664074 Irkutsk, Russia; snoei@istu.edu or noiagdams@susu.ru

⁴ Department of Applied Mathematics and Programming, South Ural State University, Lenin Prospect 76, 454080 Chelyabinsk, Russia

* Correspondence: mkalam@uoh.edu.pk

Abstract: In this paper, the 3-D squeezing flow of viscous incompressible fluid between two parallel plates rotating at the same rate is investigated. The flow is observed under the influence of the varying magnetic field. The flow phenomena are modeled by utilizing the basic governing equations, i.e., equation of continuity, coupled Navier Stokes, and Magnetic Field equations. Using appropriate similarity transformations, the resultant partial differential equations are then transformed into a system of ordinary differential equations. The computational technique is developed via the Homotopy Analysis Method (HAM) to obtain the solution of transformed systems of ordinary differential equations. The influence of several engineering fluid parameters, such as squeeze Reynolds number, magnetic field strength parameter, and magnetic Reynolds number, on velocity and magnetic field components, are observed from different graphs. It has been investigated that by increasing the squeeze Reynolds number, fluid velocity in the y and z directions will be increased as well. On the magnetic field component along the y -axis, an increasing influence of squeezing Reynolds number is also noticed. Similarly, raising the magnetic Reynolds number increases the velocity along the y -axis, whereas the inverse relationship is found for magnetic field components. Furthermore, for each flow phenomenon, an error analysis is also presented.

Keywords: MHD; Homotopy Analysis Method; heat and mass transfer; time dependent squeeze phenomenon; variable magnetic field; viscous fluid



Citation: Alam, M.K.; Bibi, K.; Khan, A.; Fernandez-Gamiz, U.; Noeiaghdam, S. The Effect of Variable Magnetic Field on Viscous Fluid between 3-D Rotatory Vertical Squeezing Plates: A Computational Investigation. *Energies* **2022**, *15*, 2473. <https://doi.org/10.3390/en15072473>

Academic Editor: Dmitry Eskin

Received: 3 February 2022

Accepted: 22 March 2022

Published: 28 March 2022

Publisher's Note: MDPI stays neutral with regard to jurisdictional claims in published maps and institutional affiliations.



Copyright: © 2022 by the authors. Licensee MDPI, Basel, Switzerland. This article is an open access article distributed under the terms and conditions of the Creative Commons Attribution (CC BY) license (<https://creativecommons.org/licenses/by/4.0/>).

1. Introduction

When a fluid is squeezed between two parallel plates approaching one other, it is called a squeeze flow. The unsteady squeezing flow between two plates rotating at different angular velocities is regarded as one of the most important study subjects due to its extensive applications in science and technology. Among these are hydrodynamic lubrication, polymer technology, biomechanics, the petroleum sector, and aerodynamic heating. The interaction of conducting fluids with electromagnetic fields is widely known as Magnetohydro Dynamics (MHD). The use of an MHD fluid as a lubricant in industrial applications is appealing because it prevents the unanticipated variation of lubricant viscosity with temperature under such high working conditions. Many experts are showing interest in this field; for example, the unsteady squeezing flow between parallel plates was considered for viscous MHD fluid by Siddiqui et al. [1]. Further, Erik Sweet [2] investigated the analytical solution for a viscous fluid flow between moving parallel plates in an unstable MHD flow.

They used the Homotopy Analysis Method to find the solution, which indicated that the magnetic field's strength has a significant impact on the flow. Later on, Murty et al. [3] observed the electrically conducting fluid in a two-phase MHD convective flow under the action of a constant transverse magnetic field through an inclined channel in a rotating system. Onyango et al. [4] experimented on an unsteady MHD flow of viscous fluid between two parallel plates under a constant pressure gradient. Khan et al. [5] observed the flow of a viscous fluid between compressing parallel plates under the influence of a varying magnetic field. They investigated the entropy generation due to magnetic fields, fluid friction, and heat transfer in a two-dimensional flow problem. Muhammad et al. [6] discussed the squeezing MHD flow between two parallel plates using Jeffrey fluid. MHD fluid flow between two parallel plates was investigated by Verma et al. [7]. Later on, Hayat et al. [8] analytically treated the squeeze flow of MHD nanofluids between two parallel plates. Furthermore, Linga Raju [9] discussed the MHD two-fluid flow of ionized gases and investigated the effect of hall current on temperature distribution. The effect of magneto-hydrodynamics on a fluid film was then observed by Hamza [10], who studied the squeezed flow between two surfaces while rotation was added to the surfaces. Unsteady Couette flow was then studied by Das et al. [11] where the flow was unsteady, and the MHD effect was added. The flow was observed in a rotating system.

A viscous fluid flow between rotating parallel plates with varying but constant angular velocities was investigated by Parter et al. [12]. In addition, [13] also added remarks on the flow when the viscous fluid is flowing between two parallel rotating plates. Further on, Rajagopal [14] also studied second ordered fluid flowing in a rotating system. Later on, the MHD double-diffusive flow of nanofluids was studied by Tripathi et al. [15], the flow was observed in a rotating channel with viscous dissipation and hall effect.

The MHD flow of viscous fluids in a rotating frame was also studied in cylindrical coordinates, as was discussed by Hughes et al. [16]. They examined the lubrication flow of such viscous fluids between rotating parallel disks. In addition, Elshekh et al. [17] talked about the film of a fluid squeezed between rotating parallel disks where an external magnetic field was applied. The influence of a changing magnetic field on the unsteady squeezing flow of viscous fluids between rotating discs was also examined by Shah et al. [18]. The squeezing unsteady flow of MHD fluid between two disks was also discussed by Ganji et al. [19], they observed the flow with suction or injection involved. Between squeezing discs moving at various velocities, the effects of MFD viscosity and magnetic field-based (MFD) thermosolutal convection of the fluid dynamics were examined by Khan et al. [20].

The unsteady squeeze flow of viscous fluids is also observed in three-dimensional rotating systems. Recently, Munawar et al. [21] studied the squeeze flow of viscous fluids in a three-dimensional rotating system. The flow was considered between parallel plates with the lower stretching plate kept porous. Further on, Alzahrani et al. [22] numerically treated the squeezed flow of viscous fluid between rotating parallel plates in a three-dimensional system and examined the effect of Dufour and Soret number. Similar work has been done on third-grade nanofluids in a three-dimensional rotating system, where the thermophoresis effect and Brownian motion were observed by Shah et al. [23]. In addition, the thin-film flow of Darcy Forchheimer hydromagnetic nanofluid between rotating parallel disks in a three-dimensional system was discussed by Riasat et al. [24]. They examined the importance of the Magnetic Reynolds number in such a system. Moreover, Fiza et al. [25] examined the flow of Jeffrey fluid in a three-dimensional rotating system. Very recently, for different fluid flow phenomena, the well-known HAM method was utilized by different authors [26–30]. They utilized the HAM method to examine the behavior of their study and predict the behavior of different problems.

The above existing literature witnessed that no study in past has been conducted so far on the 3-dimensional squeeze flow of viscous fluids between two parallel plates under the influence of the variable magnetic field, while both the plates have some angular velocity. Hence, the suggested work is the best approach toward such problems and is a way of

motivation for researchers bringing a new idea of studying the flow between unsteady rotating parallel plates.

2. Modeling and Formulation of the Physical Problem

The incompressible viscous fluid flow between two horizontal squeezing plates separated by a distance $D(t) = l(1 - \beta t)^{1/2}$ (Please see Figure 1), where l is the spacing between plates at time $t = 0$. The upper plate rotates with an angular velocity of Ω_u , whereas the lower plate moves with angular velocity Ω_l . The effect of variable magnetic field M is added externally, which produces the induced magnetic field B with the following components, B_x , B_y , and B_z .

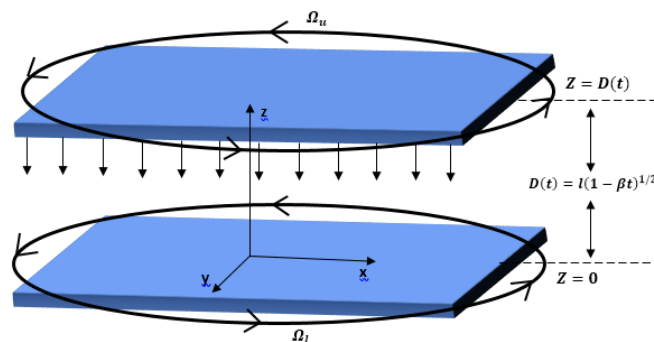


Figure 1. Geometry of the flow problem

The system of coordinates selected, is Cartesian coordinates. The origin is placed in the lower plate's center, in which the x -axis is taken along the horizontal axis and the z -axis is at a right angle to both the plates (along the vertical axis). The rotation of plates is along the y -axis. The flow between the plates occurs due to the motion of plates towards each other, i.e., the squeezing effect. The effect of gravity on the fluid is negligible. Now we observe the velocity profile of the given fluid, and the effect of the magnetic field on the velocity of fluid for these viscous fluids in a three-dimensional system. Since the coordinates of the flow are in such a way that the x -component is along the direction of the fluid and the z -component is normal to the direction of flow; thus, the component form of equation of continuity, Navier–Stokes, and magnetic field equation are, Continuity equation:

$$\frac{\partial u}{\partial x} + \frac{\partial v}{\partial y} + \frac{\partial w}{\partial z} = 0, \quad (1)$$

Navier–Stokes equation x -component:

$$\rho \left[\frac{\partial u}{\partial t} + u \frac{\partial u}{\partial x} + v \frac{\partial u}{\partial y} + w \frac{\partial u}{\partial z} \right] = -\frac{\partial P}{\partial x} + \mu \left[\frac{\partial^2 u}{\partial x^2} + \frac{\partial^2 u}{\partial y^2} + \frac{\partial^2 u}{\partial z^2} \right] + \frac{1}{\mu_2} \left[B_z \frac{\partial B_x}{\partial z} - B_z \frac{\partial B_z}{\partial x} - B_y \frac{\partial B_y}{\partial x} + B_y \frac{\partial B_x}{\partial y} \right]. \quad (2)$$

Navier–Stokes equation y -component:

$$\rho \left[\frac{\partial v}{\partial t} + u \frac{\partial v}{\partial x} + v \frac{\partial v}{\partial y} + w \frac{\partial v}{\partial z} \right] = -\frac{\partial p}{\partial y} + \mu \left[\frac{\partial^2 v}{\partial x^2} + \frac{\partial^2 v}{\partial y^2} + \frac{\partial^2 v}{\partial z^2} \right] + \frac{1}{\mu_2} \left[B_x \frac{\partial B_y}{\partial x} - B_x \frac{\partial B_x}{\partial y} - B_z \frac{\partial B_z}{\partial y} + B_z \frac{\partial B_y}{\partial z} \right]. \quad (3)$$

Navier–Stokes equation z-component:

$$\rho \left[\frac{\partial w}{\partial t} + u \frac{\partial w}{\partial x} + v \frac{\partial w}{\partial y} + w \frac{\partial w}{\partial z} \right] = -\frac{\partial p}{\partial z} + \mu \left[\frac{\partial^2 w}{\partial x^2} + \frac{\partial^2 w}{\partial y^2} + \frac{\partial^2 w}{\partial z^2} \right] + \frac{1}{\mu_2} \left[B_y \frac{\partial B_z}{\partial y} - B_y \frac{\partial B_y}{\partial z} - B_x \frac{\partial B_x}{\partial z} + B_x \frac{\partial B_z}{\partial x} \right]. \tag{4}$$

Magnetic field equation x-component:

$$\frac{\partial B_x}{\partial t} = \left[u \frac{\partial B_y}{\partial y} + B_y \frac{\partial u}{\partial y} - v \frac{\partial B_x}{\partial y} - B_x \frac{\partial v}{\partial y} - w \frac{\partial B_x}{\partial z} - B_x \frac{\partial w}{\partial z} + u \frac{\partial B_z}{\partial z} + B_z \frac{\partial u}{\partial z} \right] + \frac{1}{\delta\mu_2} \left[\frac{\partial^2 B_x}{\partial x^2} + \frac{\partial^2 B_x}{\partial y^2} + \frac{\partial^2 B_x}{\partial z^2} \right]. \tag{5}$$

Magnetic field equation y-component:

$$\frac{\partial B_y}{\partial t} = \left[v \frac{\partial B_z}{\partial z} + B_z \frac{\partial v}{\partial z} - w \frac{\partial B_y}{\partial z} - B_y \frac{\partial w}{\partial z} - u \frac{\partial B_y}{\partial x} - B_y \frac{\partial u}{\partial x} + v \frac{\partial B_x}{\partial x} + B_x \frac{\partial v}{\partial x} \right] + \frac{1}{\delta\mu_2} \left[\frac{\partial^2 B_y}{\partial x^2} + \frac{\partial^2 B_y}{\partial y^2} + \frac{\partial^2 B_y}{\partial z^2} \right]. \tag{6}$$

Magnetic field equation z-component:

$$\frac{\partial B_z}{\partial t} = \left[w \frac{\partial B_x}{\partial x} + B_x \frac{\partial w}{\partial x} - u \frac{\partial B_z}{\partial x} - B_z \frac{\partial u}{\partial x} - v \frac{\partial B_z}{\partial y} - B_z \frac{\partial v}{\partial y} + w \frac{\partial B_y}{\partial y} + B_y \frac{\partial w}{\partial y} \right] + \frac{1}{\delta\mu_2} \left[\frac{\partial^2 B_z}{\partial x^2} + \frac{\partial^2 B_z}{\partial y^2} + \frac{\partial^2 B_z}{\partial z^2} \right]. \tag{7}$$

3. Boundary Conditions

The boundary conditions for the above fluid flow are given as:

$$u = 0, v = \frac{\Omega_l x}{1 - \beta t}, w = 0, B_x = B_y = B_z = 0, \text{ at } z = 0.$$

$$u = 0, v = \frac{\Omega_u x}{1 - \beta t}, w = \frac{dD(t)}{dt}, B_x = 0, B_y = \frac{xN_0}{1 - \beta t}, B_z = \frac{-\beta M_0}{(1 - \beta t)^{1/2}},$$

at $z = D(t)$ where $D(t) = l(-\beta t)^{1/2}$.

Here, ρ is the density of fluid, P is pressure, and B is the induced magnetic field. Now, using the following transformation to convert the above partial differential equations to ordinary differential equations:

$$u = \frac{\beta x}{(1 - \beta t)} f'(\eta), v = \frac{\Omega_l x}{(1 - \beta t)} g(\eta), w = \frac{-\beta l}{(1 - \beta t)^{1/2}} f(\eta), B_x = \frac{\beta x M_0}{l(1 - \beta t)} m'(\eta),$$

$$B_y = \frac{x N_0}{(1 - \beta t)} n(\eta), B_z = \frac{-\beta M_0}{(1 - \beta t)^{1/2}} m(\eta), \eta = \frac{z}{l(1 - \beta t)^{1/2}}.$$

After non-dimensionlizing the above equations and given boundary conditions will be converted to the following O.D.E.'s:

$$f'''' = S_z \left[3f'' + (\eta - 2f)f''' - 2f'f'' \right] + 2S_z M_x^2 \left[2R_m (mm' + \eta mm'' - fmm'' + m^2 f''') - m'm'' \right], \tag{8}$$

$$g'' = S_z \left[2g + \eta g' + 2f'g - 2g'f \right] - 2S_z M_x M_y \left[m'n - n'm \right], \tag{9}$$

$$m'' = R_m \left[m + \eta m' - 2m'f + 2f'm \right], \tag{10}$$

$$n'' = R_m \left[2n + \eta n' - 2n' f + 2f' n - 2 \left(\frac{M_x}{M_y} \right) (g' m - m' g) \right], \tag{11}$$

where $S_z = \frac{\beta l^2}{2\nu}$, denotes the Squeezing Reynolds number, $M_x = \frac{M_0}{l\sqrt{\rho\mu_2}}$, represents the Magnetic field strength along the x -axis, $M_y = \frac{N_0}{\Omega_l\sqrt{\rho\mu_2}}$ is the Magnetic field strength along x -axis and $R_m = S_z B_t$ which is given by, $R_m = \left(\frac{\beta l^2}{2\nu} \right) (\nu\sigma\mu_2)$ is the Magnetic Reynolds number, and the boundary conditions become of the form:

$$\begin{aligned} f(0) = 0, f'(0) = 0, g(0) = 1, m(0) = 0, n(0) = 0. \\ f(1) = \frac{1}{2}, f'(1) = 0, g(1) = \frac{\Omega_u}{\Omega_l} = S, m(1) = 1, n(1) = 1. \end{aligned}$$

4. Method of Solution

An analytical technique was used to find the solution of Equations (8)–(11), known as the Homotopy Analysis Method. We express the functions $f, g, m,$ and n (where $f, g, m,$ and n are the functions of $\eta, \eta^K, K \geq 0$) as a set of base functions:

$$f_n = \sum_{K=0}^{\infty} a_K \eta^K \tag{12}$$

$$g_n = \sum_{K=0}^{\infty} b_K \eta^K \tag{13}$$

$$m_n = \sum_{K=0}^{\infty} c^K \eta^K \tag{14}$$

$$n_n = \sum_{K=0}^{\infty} d^K \eta^K \tag{15}$$

where the constant co-efficients $a_K, b_K, c_K,$ and d_k are to be determined. Initial approximations are chosen as follows:

$$f_0 = 1.5 * \eta^2 - \eta^3; \tag{16}$$

$$g_0 = (S - 1) * \eta + 1; \tag{17}$$

$$m_0 = \eta; \tag{18}$$

$$n_0 = \eta \tag{19}$$

now to choose the auxiliary operators:

$$\mathcal{L}_f = \frac{\partial^4}{\partial \eta^4}, \mathcal{L}_g = \frac{\partial^2}{\partial \eta^2}, \mathcal{L}_m = \frac{\partial^2}{\partial \eta^2}, \mathcal{L}_n = \frac{\partial^2}{\partial \eta^2} \tag{20}$$

with the following properties

$$\mathcal{L}_f(k_1 * \eta^3 + K_2 * \eta^2 + K_3 * \eta + K_4 *) = 0 \tag{21}$$

$$\mathcal{L}_g(K_5 * \eta + K_6 *) = 0 \tag{22}$$

$$\mathcal{L}_m(K_7 * \eta + K_8 *) = 0 \tag{23}$$

$$\mathcal{L}_n(K_9 * \eta + K_{10} *) = 0 \tag{24}$$

where $K_1*, K_2*, K_3*, K_4*, K_5*, K_6*, K_7*, K_8*, K_9*,$ and $K_{10}*$ are arbitrary constants.

We can obtain the Zeroth order deformation as:

$$(1 - s)\mathcal{L}_f[f(\eta; s) - f_0(\eta)] = s\hbar_f\mathfrak{N}_f[f(\eta; s), m(\eta; s)] \tag{25}$$

$$(1 - s)\mathcal{L}_g[g(\eta; s) - g_0(\eta)] = s\hbar_g\mathfrak{N}_g[f(\eta; s), g(\eta; s), m(\eta; s), n(\eta; s)] \tag{26}$$

$$(1 - s)\mathcal{L}_m[m(\eta; s) - m_0(\eta)] = s\hbar_m\mathfrak{N}_m[f(\eta; s), m(\eta; s)] \tag{27}$$

$$(1 - s)\mathcal{L}_n[n(\eta; s) - n_0(\eta)] = s\hbar_n\mathfrak{N}_n[f(\eta; s), g(\eta; s), m(\eta; s), n(\eta; s)] \tag{28}$$

From Equations (14)–(17), the nonlinear operators are define as:

$$\begin{aligned} \mathfrak{N}_f[f(\eta; s), m(\eta; s)] &= \frac{\partial^4 f(\eta; s)}{\partial \eta^4} - S_z \left(3 \frac{\partial^2 f(\eta; s)}{\partial \eta^2} + (\eta - 2f) \frac{\partial^3 f(\eta; s)}{\partial \eta^3} \right. \\ &\quad \left. - 2 \frac{\partial f(\eta; s)}{\partial \eta} \frac{\partial^2 f(\eta; s)}{\partial \eta^2} \right) - 2S_z M_x^2 \\ &\quad \left(M \frac{\partial^3 M(\eta; s)}{\partial \eta^3} - \frac{\partial M(\eta; s)}{\partial \eta} \frac{\partial^2 M(\eta; s)}{\partial \eta^2} \right) \end{aligned} \tag{29}$$

$$\begin{aligned} \mathfrak{N}_g[f(\eta; s), g(\eta; s), m(\eta; s), n(\eta; s)] &= \frac{\partial^2 g(\eta; s)}{\partial \eta^2} - S_z \left(2g + \eta \frac{\partial g(\eta; s)}{\partial \eta} + 2 \frac{\partial f(\eta; s)}{\partial \eta} g \right. \\ &\quad \left. - 2 \frac{\partial g(\eta; s)}{\partial \eta} f \right) - 2S_z M_x M_y \\ &\quad \left(\frac{\partial m(\eta; s)}{\partial \eta} n - m \frac{\partial n(\eta; s)}{\partial \eta} \right) \end{aligned} \tag{30}$$

$$\begin{aligned} \mathfrak{N}_m[f(\eta; s), m(\eta; s)] &= \frac{\partial^2 m(\eta; s)}{\partial \eta^2} - R_m \left(m + \eta \frac{\partial m(\eta; s)}{\partial \eta} - 2 \right. \\ &\quad \left. \left(f \frac{\partial m(\eta; s)}{\partial \eta} - m \frac{\partial f(\eta; s)}{\partial \eta} \right) \right) \end{aligned} \tag{31}$$

$$\begin{aligned} \mathfrak{N}_n[f(\eta; s), g(\eta; s), m(\eta; s), n(\eta; s)] &= \frac{\partial^2 n(\eta; s)}{\partial \eta^2} - R \left(2n + \eta \frac{\partial n(\eta; s)}{\partial \eta} \right. \\ &\quad \left. - 2 \left(\frac{\partial n(\eta; s)}{\partial \eta} f - n \frac{\partial f(\eta; s)}{\partial \eta} \right) + 2 \frac{\partial M_x}{\partial M_y} \right. \\ &\quad \left. \left(\frac{\partial g(\eta; s)}{\partial \eta} m - g \frac{\partial m(\eta; s)}{\partial \eta} \right) \right) \end{aligned} \tag{32}$$

where s is a fixed parameter, nonlinear parameters are $\mathfrak{N}_f, \mathfrak{N}_g, \mathfrak{N}_m$ and \mathfrak{N}_n , while $\hbar_f, \hbar_g, \hbar_m$, and \hbar_n are the nonzero auxiliary parameters.

For $s = 0$ and $s = 1$, we have:

$$\begin{aligned} f(\eta, 0) &= f_0, & f(\eta, 1) &= f(\eta) \\ g(\eta, 0) &= g_0, & g(\eta, 1) &= g(\eta) \\ m(\eta, 0) &= m_0, & m(\eta, 1) &= m(\eta) \\ n(\eta, 0) &= n_0, & n(\eta, 1) &= n(\eta) \end{aligned} \tag{33}$$

as s varies from 0 to 1, exact solutions of $f(\eta)$, $g(\eta)$, $n(\eta)$, and $n(\eta)$ can be obtained from initial guesses of f_0, g_0, m_0 , and n_0 , respectively.

For these functions, the Taylor’s series are given by:

$$f(\eta; s) = f_0 + \sum_{n=1}^{\infty} q^n f_n(\eta) \tag{34}$$

$$g(\eta; s) = g_0 + \sum_{n=1}^{\infty} q^n g_n(\eta) \tag{35}$$

$$m(\eta; s) = m_0 + \sum_{n=1}^{\infty} q^n m_n(\eta) \tag{36}$$

$$n(\eta; s) = n_0 + \sum_{n=1}^{\infty} q^n n_n(\eta) \tag{37}$$

$$\begin{aligned} f_n(\eta) &= \left. \frac{1}{n!} \frac{\partial^n f(\eta; s)}{\partial \eta^n} \right|_{s=0}, & g_n(\eta) &= \left. \frac{1}{n!} \frac{\partial^n g(\eta; s)}{\partial \eta^n} \right|_{s=0} \\ m_n(\eta) &= \left. \frac{1}{n!} \frac{\partial^n m(\eta; s)}{\partial \eta^n} \right|_{s=0}, & n_n(\eta) &= \left. \frac{1}{n!} \frac{\partial^n n(\eta; s)}{\partial \eta^n} \right|_{s=0} \end{aligned} \tag{38}$$

It can be noted that in the above series convergence strongly depends upon $\hbar_f, \hbar_g, \hbar_m,$ and \hbar_n .

Assuming that these nonzero auxiliary parameters are chosen so that the equations converge at $s = 1$, one can obtain:

$$f(\eta) = f_0 + \sum_{n=1}^{\infty} f_n(\eta) \tag{39}$$

$$g(\eta) = g_0 + \sum_{n=1}^{\infty} g_n(\eta) \tag{40}$$

$$m(\eta) = m_0 + \sum_{n=1}^{\infty} m_n(\eta) \tag{41}$$

$$n(\eta) = n_0 + \sum_{n=1}^{\infty} n_n(\eta) \tag{42}$$

Differentiating the Equations (28)–(31) n -times with respect to s and putting $s = 0$, we have:

$$\mathcal{L}_f[f_n(\eta) - \chi_n f_{n-1}(\eta)] = \hbar_f R_{f,n}(\eta) \tag{43}$$

$$\mathcal{L}_g[g_n(\eta) - \chi_n g_{n-1}(\eta)] = \hbar_g R_{g,n}(\eta) \tag{44}$$

$$\mathcal{L}_m[m_n(\eta) - \chi_n m_{n-1}(\eta)] = \hbar_m R_{m,n}(\eta) \tag{45}$$

$$\mathcal{L}_n[n_n(\eta) - \chi_n n_{n-1}(\eta)] = \hbar_n R_{n,n}(\eta) \tag{46}$$

with the given boundary conditions,

$$\begin{aligned} f_n(0) = 0, & \quad f'_n(0) = 0, & g_n(0) = 1, & \quad m_n(0) = 0, & \quad n_n(0) = 0 \\ f_n(1) = 0.5, & \quad f'_n(1) = 0, & g_n(1) = S, & \quad m_n(1) = 1, & \quad n_n(1) = 1 \end{aligned} \tag{47}$$

$$\begin{aligned} R_{f,n}(\eta) &= f''''_{n-1}(\eta) - S_z \left(3f''_{n-1}(\eta) + (\eta)f'''_{n-1}(\eta) - 2f'_{n-1}(\eta)f''_{n-1}(\eta) \right. \\ &\quad \left. - 2 \sum_{j=0}^{n-1} f_j(\eta)f''_{n-j-1}(\eta) \right) + 2S_z M_x^2 \left(2R_m \sum_{j=0}^{n-1} m_j(\eta) \left[m'_{n-j-1}(\eta) \right. \right. \\ &\quad \left. \left. + \eta m''_{n-j-1}(\eta) + m_{n-j-1}(\eta)f''_{n-j-1}(\eta) \right] - m'_{n-1}(\eta)m''_{n-1}(\eta) \right) \end{aligned} \tag{48}$$

$$R_{g,n}(\eta) = g''_{n-1}(\eta) - S_z \left(2g_{n-1}(\eta) + (\eta)g'_{n-1}(\eta) + 2 \sum_{j=0}^{n-1} \left[g_j(\eta)f'_{n-j-1}(\eta) - f_j(\eta)g'_{n-j-1}(\eta) \right] + 2S_z M_x M_y \right. \\ \left. \sum_{j=0}^{n-1} \left(n_j(\eta)m'_{n-j-1}(\eta) - n_{j(\eta)}m'_{n-j-1}(\eta) \right) \right) \quad (49)$$

$$R_{m,n}(\eta) = m''_{n-1}(\eta) - R_m \left[m_{n-1}(\eta) + (\eta)m'_{n-1}(\eta) + 2 \sum_{j=0}^{n-1} \left(m_j(\eta)f'_{n-j-1}(\eta) - f_j(\eta)m'_{n-j-1}(\eta) \right) \right] \quad (50)$$

$$R_{n,n}(\eta) = n''_{n-1}(\eta) - R_m \left[2n_{n-1}(\eta) + (\eta)n'_{n-1}(\eta) + 2 \sum_{j=0}^{n-1} \left(n_j(\eta)f'_{n-j-1}(\eta) - f_j(\eta)n'_{n-j-1}(\eta) \right) - 2 \frac{M_x}{M_y} \left(m_j(\eta)g'_{n-j-1}(\eta) - g_j(\eta)m'_{n-j-1}(\eta) \right) \right] \quad (51)$$

and $\chi_n = \{1, \text{ if } n > 1, \text{ and } 0, \text{ if } n = 1\}$.

Finally, the general solution of (41–43) can be written as:

$$f_n(\eta) = \int_0^\eta \int_0^\eta \int_0^\eta \int_0^\eta \hbar_f R_{f,n}(z) dz dz dz dz + \chi_n f_{n-1} + K_{1*} \eta^3 + K_{2*} \eta^2 + K_{3*} \eta + K_{4*} \quad (52)$$

$$g_n(\eta) = \int_0^\eta \int_0^\eta \hbar_g R_{g,n}(z) dz dz + \chi_n g_{n-1} + K_{5*} \eta + K_{6*} \quad (53)$$

$$m_n(\eta) = \int_0^\eta \int_0^\eta \hbar_m R_{m,n}(z) dz dz + \chi_n m_{n-1} + K_{7*} \eta + K_{8*} \quad (54)$$

$$n_n(\eta) = \int_0^\eta \int_0^\eta \hbar_n R_{n,n}(z) dz dz + \chi_n n_{n-1} + K_{9*} \eta + K_{10*} \quad (55)$$

and so for $f(\eta)$, $g(\eta)$, $m(\eta)$, and $n(\eta)$, the exact solution becomes:

$$f(\eta) \approx \sum_{m=0}^n f_m(\eta) \\ g(\eta) \approx \sum_{m=0}^n g_m(\eta) \\ m(\eta) \approx \sum_{m=0}^n m_m(\eta) \\ n(\eta) \approx \sum_{m=0}^n n_m(\eta). \quad (56)$$

5. Optimal Convergence Control Parameters

It should be noted that the nonzero auxiliary parameters \hbar_f , \hbar_g , \hbar_m , and \hbar_n contained in the series solutions (41–43), through which the rate of the homotopy series solutions and convergence region can be determined. Average residual errors were used to obtain the optimal values of \hbar_f , \hbar_g , \hbar_m , and \hbar_n :

$$\varepsilon_n^f = \frac{1}{K+1} \sum_{j=0}^K \left[\mathfrak{N}_f \left(\sum_{i=0}^n f(\eta), \sum_{i=0}^n m(\eta) \right)_{m=j\delta m} \right]^2 d\eta \quad (57)$$

$$\epsilon_n^g = \frac{1}{K+1} \sum_{j=0}^K \left[\mathfrak{N}_g \left(\sum_{i=0}^n f(\eta), \sum_{i=0}^n g(\eta), \sum_{i=0}^n m(\eta), \sum_{i=0}^n n(\eta) \right)_{m=j\delta m} \right]^2 d\eta \tag{58}$$

$$\epsilon_n^m = \frac{1}{K+1} \sum_{j=0}^K \left[\mathfrak{N}_m \left(\sum_{i=0}^n f(\eta), \sum_{i=0}^n m(\eta) \right)_{m=j\delta m} \right]^2 d\eta \tag{59}$$

$$\epsilon_n^n = \frac{1}{K+1} \sum_{j=0}^K \left[\mathfrak{N}_n \left(\sum_{i=0}^n f(\eta), \sum_{i=0}^n g(\eta), \sum_{i=0}^n m(\eta), \sum_{i=0}^n n(\eta) \right)_{m=j\delta m} \right]^2 d\eta \tag{60}$$

Furthermore,

$$\epsilon_n^t = \epsilon_n^f + \epsilon_n^g + \epsilon_n^m + \epsilon_n^n \tag{61}$$

where the total squared residual error is ϵ_n^t . We can minimize the total average squared residual error by applying the Mathematica package BVPh 2.0. To acquire the local optimal convergence control parameters, the command Minimize was used.

6. Error Analysis

Taking 10^{-40} as a maximum residual error, the problem was solved with the HAM BVPh 2.0 package. An investigation was made using 40th-order approximations. The provision of error analysis supports the authentication of results for many relevant physical parameters in Figure 2 and from results given in Table 1.

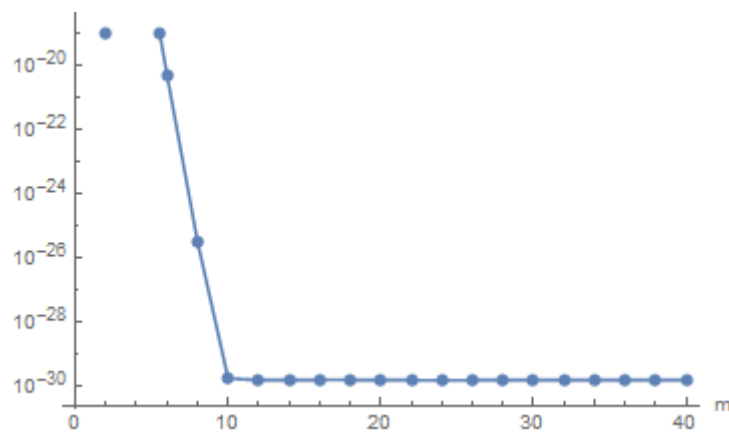


Figure 2. Total residual error, with $S_z = -0.1$, $M_x = 0.1$, $M_y = 0.3$, $R_m = 0.01$, and $S = 1$.

Table 2 is provided to determine the equations' inaccuracy from the Navier–Stokes and magnetic field equations. An increase in the order of approximation can be seen, the solution obtained from these equations converges to the exact analysis.

Table 1. Estimating the total residual error with fixed values of $S_z = -0.1$, $M_x = 0.1$, $M_y = 0.3$, $R_m = 0.01$, and $S = 1$, for different orders of approximations.

m	ϵ_m^f	ϵ_m^g	ϵ_m^m	ϵ_m^n	CPU Time
1	5.56818×10^{-7}	1.50838×10^{-5}	2.75325×10^{-8}	3.42075×10^{-8}	0.42 s
5	1.04968×10^{-24}	4.31742×10^{-19}	7.60909×10^{-23}	1.89839×10^{-18}	4.19 s
10	1.48326×10^{-30}	9.10580×10^{-33}	1.64090×10^{-35}	4.81645×10^{-34}	18.5 s
15	1.47350×10^{-30}	9.86847×10^{-33}	1.86358×10^{-35}	1.38805×10^{-35}	33.5 s
20	1.48626×10^{-30}	9.78372×10^{-33}	1.79738×10^{-35}	1.50240×10^{-35}	61.6 s
25	1.47036×10^{-30}	9.78372×10^{-33}	1.79738×10^{-35}	1.48434×10^{-35}	106.08 s
30	1.47036×10^{-30}	9.78372×10^{-33}	1.79738×10^{-35}	1.48434×10^{-35}	163.13 s
35	1.47036×10^{-30}	9.78372×10^{-33}	1.79738×10^{-35}	1.48434×10^{-35}	240.95 s
40	1.47036×10^{-30}	9.78372×10^{-33}	1.79738×10^{-35}	1.48434×10^{-35}	456.57 s

Table 2. With fixed values of $S_z = -0.1, M_x = 0.1, M_y = 0.3, R_m = 0.01, S = 1$, observing the optimal values of convergence control parameters in comparison to different orders of approximation.

Order	h_f	h_g	h_m	h_n	ϵ_m^t
2	-1.00242	-1.02522	-0.99578	-1.01863	7.07983×10^{-9}
3	-1.00597	-1.02361	-0.98895	-1.00881	3.11944×10^{-12}
4	-1.00854	-1.02152	-0.98596	-1.01663	1.17465×10^{-15}
5	-1.02616	-1.03854	-0.96740	-0.97698	-3.79267×10^{-15}
6	-0.93502	-1.07429	-1.07428	-0.94309	2.53023×10^{-14}
7	-0.89878	-0.95454	-1.09525	-0.90992	3.93815×10^{-14}

The total residual error is represented in Table 1 and graphically through Figure 2, for different orders of approximation. These results show that at the 25th order of approximation, the solution converges where the error almost reduces continuously. With the fixed values of parameters, $S_z = -0.1, M_x = 0.1, M_y = 0.3, R_m = 0.01$, and $S = 1$. With fixed values of $S_z = -0.1, M_x = 0.1, M_y = 0.3, R_m = 0.01$, and $S = 1$, Table 2, shows the optimal values of convergence control parameters for various approximation orders. Table 3, shows the estimated values of $f(\eta), g(\eta), m(\eta)$, and $n(\eta)$ at different values of η . These results show that the solution is accurate by verification through the given boundary conditions of the problem (since the boundary conditions can be verified by observing the obtained numerical values at different points). Table 4 shows the convergence of the HAM solution for different orders of approximation for the skin-friction, i.e., for $f''(0), -g'(0), -m'(0)$, and $-n'(0)$, with $S_z = -0.1, M_x = 0.5, M_y = 0.3, R_m = 0.01$, and $S = 1$. It can be observed that the solution is convergent for the 10th order of approximation. The analysis is carried out up to the 40th order of approximation.

Table 3. Estimated values for $f(\eta), g(\eta), m(\eta)$, and $n(\eta)$, by fixing $S_z = -0.1, M_x = 0.1, M_y = 0.3, R_m = 0.01, S = 1$, and different values of η .

η	$f(\eta)$	$g(\eta)$	$m(\eta)$	$n(\eta)$
0.	0.	1.	0.	0.
0.1001	0.013999	1.014380	0.099721	0.099865
0.2002	0.052032	1.026218	0.199465	0.199696
0.3003	0.108119	1.034940	0.299257	0.299529
0.4004	0.176245	1.040324	0.399126	0.399401
0.5005	0.250378	1.042131	0.499097	0.499346
0.6006	0.324481	1.040296	0.599192	0.599396
0.7007	0.392515	1.034878	0.699428	0.699577
0.8008	0.448449	1.026084	0.799814	0.799904
0.9009	0.486271	1.014256	0.900345	0.900383
1.	0.5	1.	1.	1.

Table 4. For different orders of approximation for $f''(0), -g'(0), -m'(0)$, and $-n'(0)$, evaluating the convergence of the HAM solution with fixed values of $S_z = -0.1, M_x = 0.5, M_y = 0.3, R_m = 0.01$, and $S = 1$.

m	$f''(0)$	$-g'(0)$	$-m'(0)$	$-n'(0)$
1	2.990612172696	-0.153255933196	-0.996111208570	-1.011230294203
5	2.990713652636	-0.154752127452	-0.996176676870	-1.011568276329
10	2.990713652641	-0.154752127484	-0.996176676875	-1.011568276329
15	2.990713652641	-0.154752127484	-0.996176676875	-1.011568276329
20	2.990713652641	-0.154752127484	-0.996176676875	-1.011568276329
25	2.990713652641	-0.154752127484	-0.996176676875	-1.011568276329
30	2.990713652641	-0.154752127484	-0.996176676875	-1.011568276329
35	2.990713652641	-0.154752127484	-0.996176676875	-1.011568276329
40	2.990713652641	-0.154752127484	-0.996176676875	-1.011568276329

Tables 5–8, shows the numerical results for $f''(0)$, $-g'(0)$, $-m'(0)$, and $-n'(0)$ by varying S_z , M_x , M_y , and R_m , respectively. This shows that increasing the squeeze parameter S_z , results in a decrease in the value of $f''(0)$ and $-m'(0)$, while oppositely $-g'(0)$ and $-n'(0)$ increases with increasing S_z . Similarly, for increasing M_x , there is a gradual increase in the values of $f''(0)$, $-g'(0)$, and $-m'(0)$, while the values of $-n'(0)$ show a gradual decrease. In Table 6, the increasing values of M_y show a certain decreasing effect on both $-g'(0)$ and $-n'(0)$, while the effects on $f''(0)$ and $-m'(0)$ are negligible. Table 7 depicts the impact of the magnetic Reynolds numbers of the skin friction, showing that with an increase in the values of R_m , the values of $-g'(0)$ and $-n'(0)$ increase gradually, but on the other hand, $f''(0)$ and $-m'(0)$ decreases.

Table 5. Estimated values for $f''(0)$, $-g'(0)$, $-m'(0)$, and $-n'(0)$ with fixed $M_x = 0.5$, $M_y = 0.3$, $R_m = 0.01$, $S = 1$, and different values of S_z .

S_z	$f''(0)$	$-g'(0)$	$-m'(0)$	$-n'(0)$
−0.1	2.990713	−0.154752	−0.996176	−1.011568
−0.5	2.953293	−0.888098	−0.996174	−1.013783
−0.75	2.929678	−1.472508	−0.996172	−1.015593
−1.1	2.896317	−2.546940	−0.996170	−1.018992

Table 6. Estimated values for $f''(0)$, $-g'(0)$, $-m'(0)$, and $-n'(0)$ with fixed $S_z = -0.1$, $M_y = 0.3$, $R_m = 0.01$, $S = 1$, and different values of M_x .

M_x	$f''(0)$	$-g'(0)$	$-m'(0)$	$-n'(0)$
0.1	2.990701	−0.154715	−0.996177	−0.997930
0.5	2.990713	−0.154752	−0.996177	−1.011568
1	2.990753	−0.154882	−0.996177	−1.028616
1.5	2.990818	−0.155101	−0.996177	−1.045666

Table 7. Estimated values for $f''(0)$, $-g'(0)$, $-m'(0)$, and $-n'(0)$ with fixed $S_z = -0.1$, $M_x = 0.5$, $R_m = 0.01$, $S = 1$, and different values of M_y .

M_y	$f''(0)$	$-g'(0)$	$-m'(0)$	$-n'(0)$
1	2.990713	−0.154740	−0.996177	−0.999635
3	2.990713	−0.154705	−0.996177	−0.996226
5	2.990713	−0.154670	−0.996177	−0.995544
7	2.990713	−0.154635	−0.996177	−0.995252

Table 8. Estimated values for $f''(0)$, $-g'(0)$, $-m'(0)$, and $-n'(0)$ with fixed $S_z = -0.1$, $M_x = 0.5$, $M_y = 0.3$, $S = 1$, and different values of R_m .

R_m	$f''(0)$	$-g'(0)$	$-m'(0)$	$-n'(0)$
0.1	2.990819	−0.155092	−0.962698	−1.110618
0.5	2.991071	−0.156280	−0.831865	−1.456702
1	2.991040	−0.157259	−0.701194	−1.729091
1.5	2.990777	−0.157899	−0.597468	−1.883300

Furthermore, Figure 3 represents the error profile for different velocity and magnetic field components, i.e., $f(\eta)$, $g(\eta)$, $m(\eta)$, and $n(\eta)$. Meanwhile, a 3-dimensional profile for the velocity components and the magnetic field components are represented in Figure 4. Showing that flow variables are satisfying the given boundary conditions.

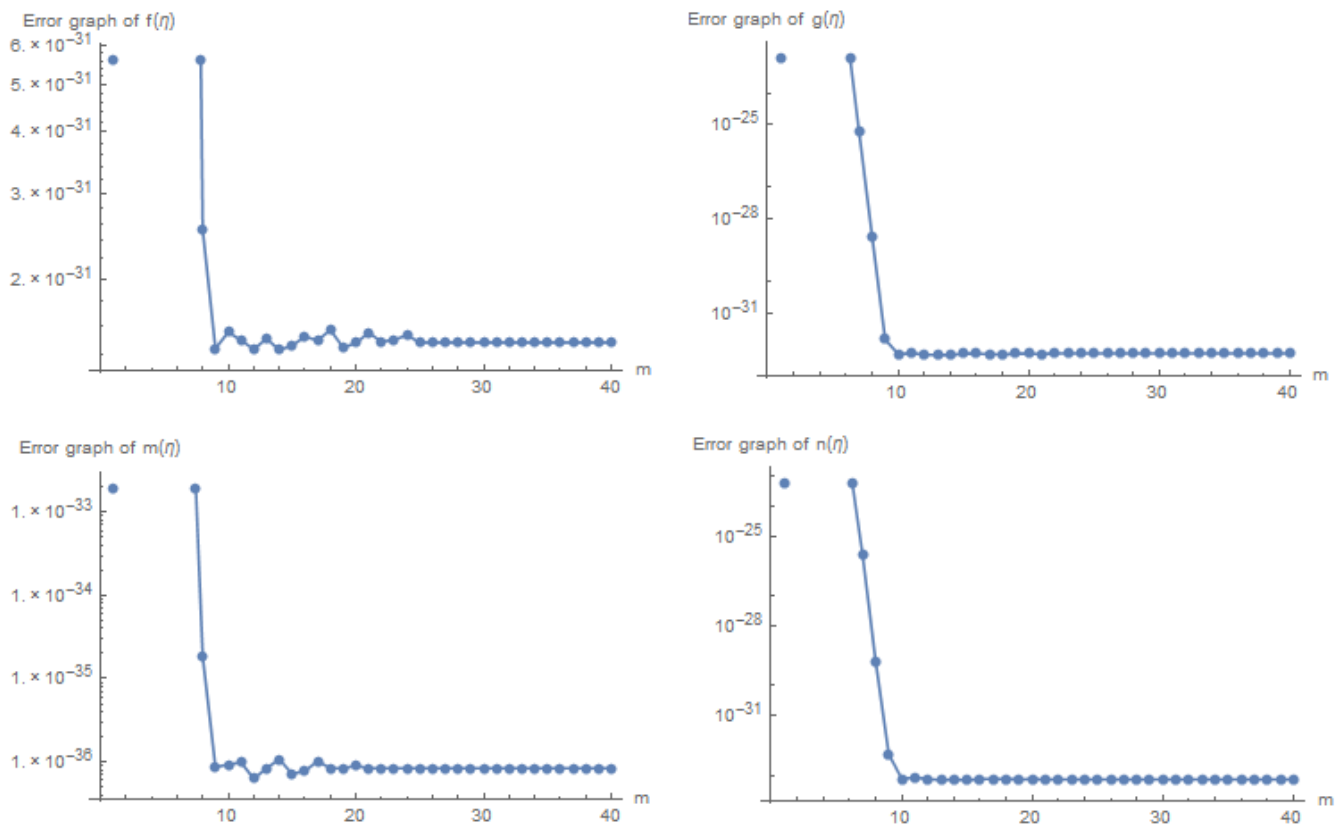


Figure 3. Error profile for $f(\eta)$, $g(\eta)$, $m(\eta)$, and $n(\eta)$, with fixed $S_z = -0.1$, $M_x = 0.1$, $M_y = 0.3$, $R_m = 0.01$, and $S = 1$.

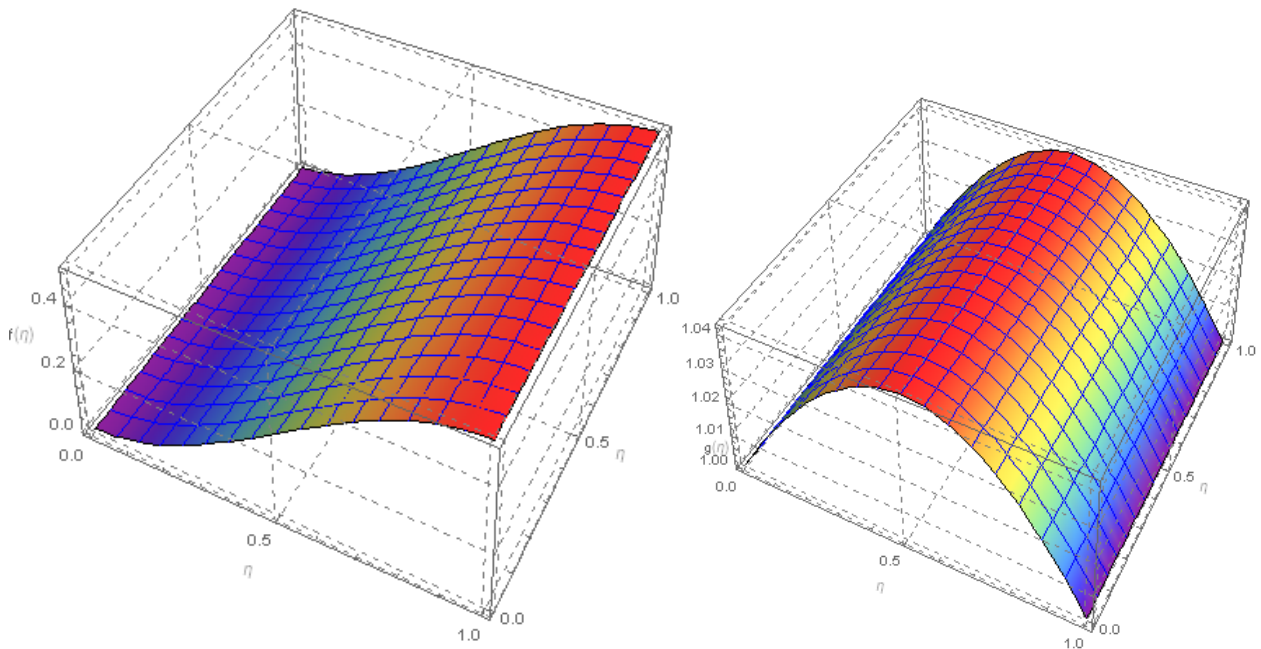


Figure 4. Cont.

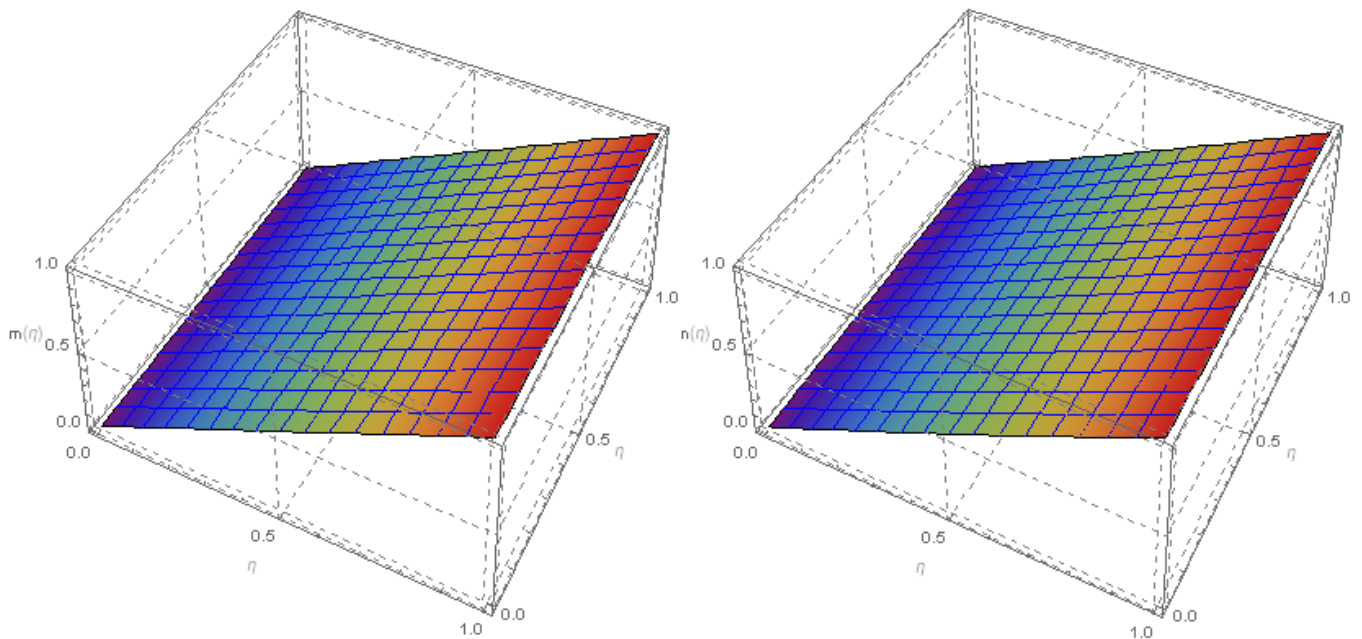


Figure 4. 3D graph for $f(\eta)$, $g(\eta)$, $m(\eta)$, and $n(\eta)$ with $S_z = -0.1$, $M_x = 0.1$, $M_y = 0.3$, $R_m = 0.01$, and $S = 1$.

7. Results and Discussion

In this section, the effects of the different involved flow parameters are discussed graphically on velocity and magnetic field components. The effects of squeezing the Reynolds numbers can be depicted from Figures 5–7. It is observed that for fixed values of the other parameters, i.e., M_x , M_y , R_m , and S . It is clear that increasing the squeeze Reynolds number (moving upper disc towards lower disc with increasing order pattern) has a direct effect on the velocity components in both the y - and z -directions. Meanwhile, in the x -direction, the velocity increases initially but shows a decreasing effect as $\eta \rightarrow 1$. Where, as in the case of magnetic field, the increase in squeeze Reynolds number results in a decrease in the magnetic field component along the z -direction, while a direct relation is observed for the y -component of the magnetic field, i.e., increasing the squeeze number causes an increase in the magnetic field along the y -direction.

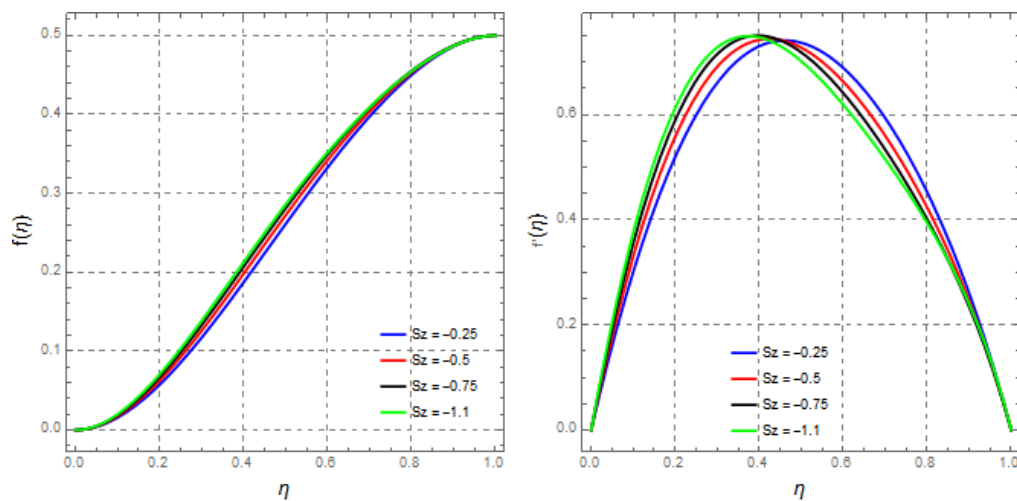


Figure 5. Impact of squeeze Reynolds number S_z on the velocity component f and f' , keeping $M_x = -3.25$, $M_y = 10$, $R_m = -0.75$, and $S = 1$.

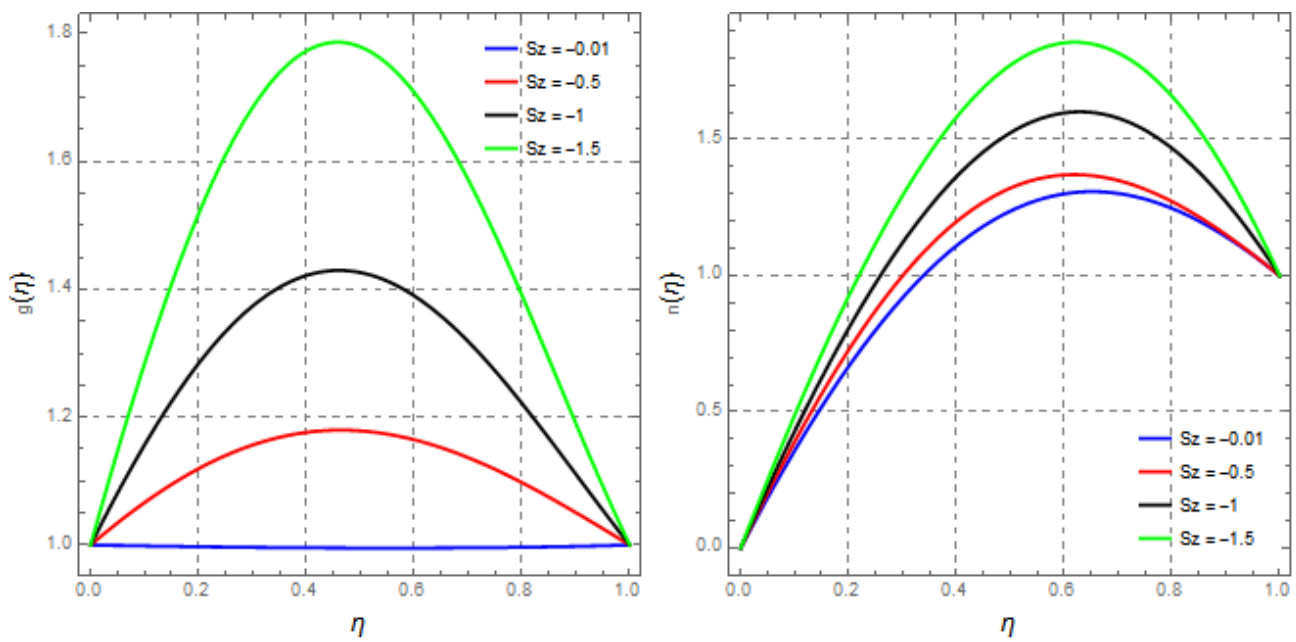


Figure 6. Impact of squeeze Reynolds number S_z on velocity component g and n , keeping $M_x = -1$, $M_y = 0.5$, $R_m = -0.75$, and $S = 1$.

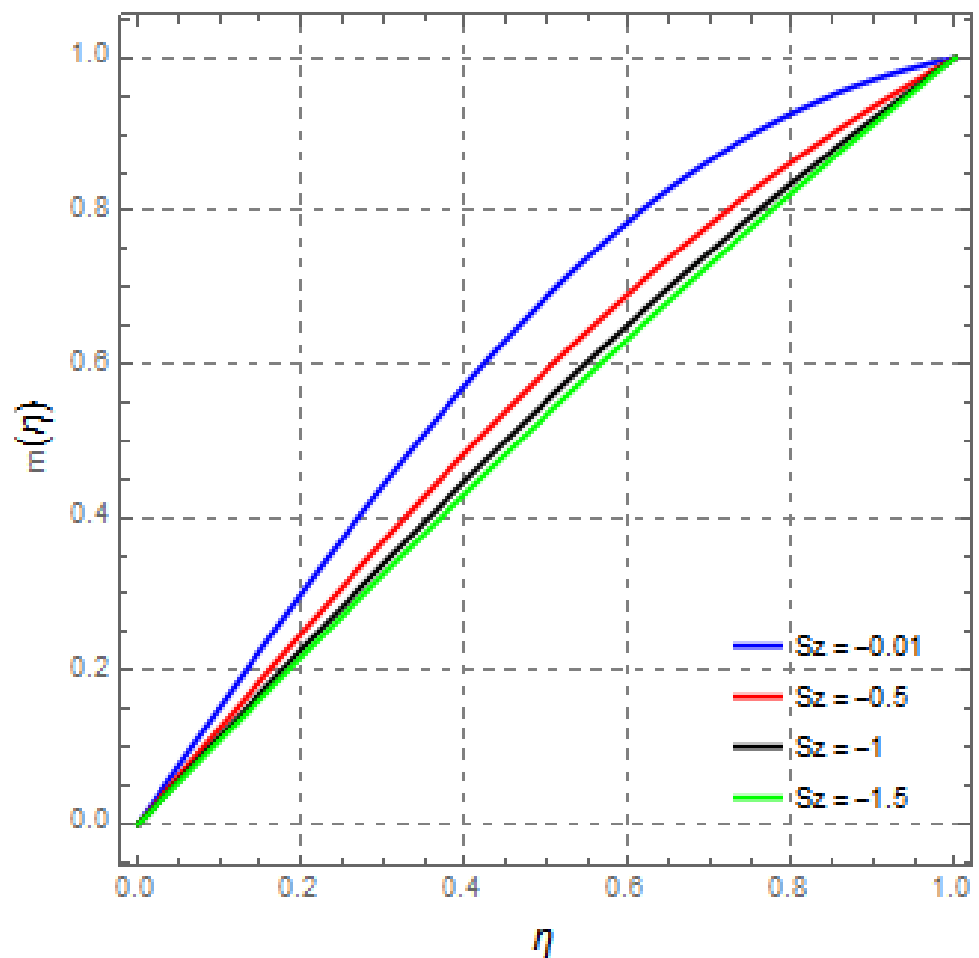


Figure 7. Impact of squeeze Reynolds number S_z on the magnetic field component m , keeping $M_x = -1.5$, $M_y = 0.5$, $R_m = -1$, and $S = 1$.

The magnetic field strength M_x is the dimensionless axial strength of the magnetic field. For fixed values of other parameters, from Figures 8–11, it is observed that an increase in M_x causes an increase in the velocity component $f(\eta)$, but a decrease in the velocity component $g(\eta)$ was found with an increasing magnetic field strength along the x -component. For the velocity component $f'(\eta)$, it was observed that the initial velocity along the x -component increased with the increasing magnetic field strength, but starts decreasing as $\eta \rightarrow 1$. Further on, a decreasing effect of M_x in the magnetic field component m can be depicted from the figure. However, in the case of the magnetic field component $n(\eta)$, a direct relation could be seen. The impact of the magnetic field strength M_y is observed from Figure 12, which is the strength of the magnetic field in the y -direction. It was found that both the velocity $g(\eta)$ and the magnetic field component $n(\eta)$ decrease with an increase in magnetic field strength, i.e., an inverse relation was observed in both cases.

To observe the effects of the magnetic Reynolds number R_m , Figures 13–15 illustrate the relations. As can be seen from the figures, with the fixed values of other parameters, increasing the magnetic Reynolds number caused a decrease in the velocity component f , but an increase in the velocity component $g(\eta)$ was observed, while increasing R_m , which led to an increase in the value of shear force due to the non-uniform distribution of the body force. Body force accelerates near the relative core wall layer because the Lorentz force is small near the squeezed plate (because of the current being almost parallel to the magnetic field). For the x -component of velocity, a decrease in the velocity occurred initially, but started increasing as $\eta \rightarrow 1$, the maximum value of f' was observed at the center. In the case of the magnetic field component $m(\eta)$ for $R_m = 0.1$, the almost linear profile was observed. Meanwhile, increasing the value of R_m , the profile became parabolic. Furthermore, it is shown that by increasing R_m , the profile for $m(\eta)$ decreases. Similarly, an inverse relationship was observed in the case of the magnetic field component $n(\eta)$, i.e., when increasing the values of R_m , the profile of $n(\eta)$ decreases. Similarly, for larger values of R_m , the profile becomes more parabolic.

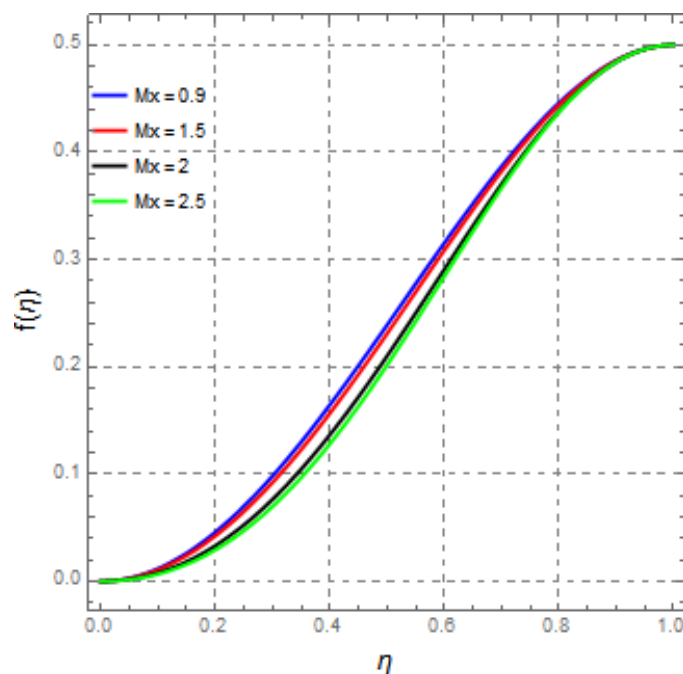


Figure 8. Impact of magnetic field strength M_x on the velocity component f , keeping $S_z = -2$, $M_y = 3$, $R_m = 1$, and $S = 1$.

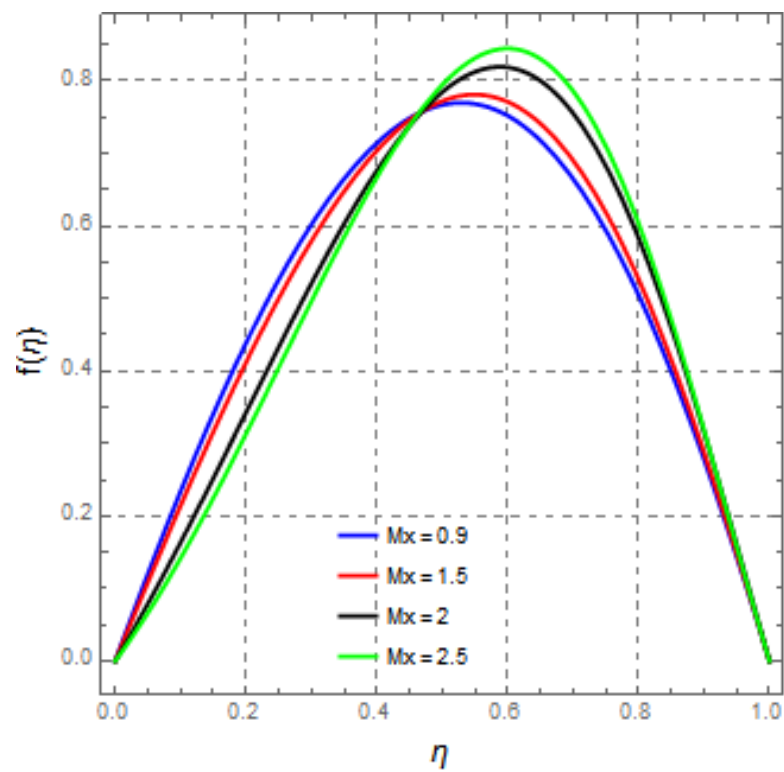


Figure 9. Impact of magnetic field strength M_x on velocity component f' , keeping $S_z = -2$, $M_y = 3$, $R_m = 1$, and $S = 1$.

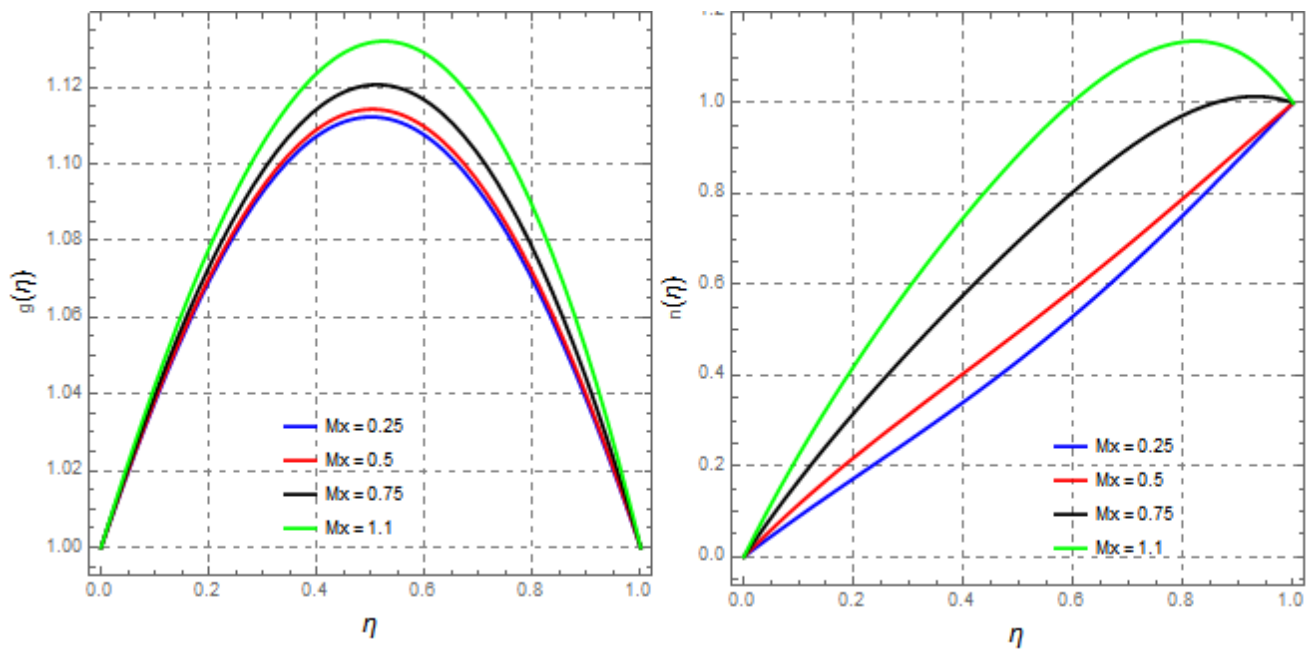


Figure 10. Impact of Magnetic field strength M_x on velocity component g and magnetic field component n , Keeping $S_z = -0.25$, $M_y = 3$, $R_m = 0.5$ and $S = 1$.

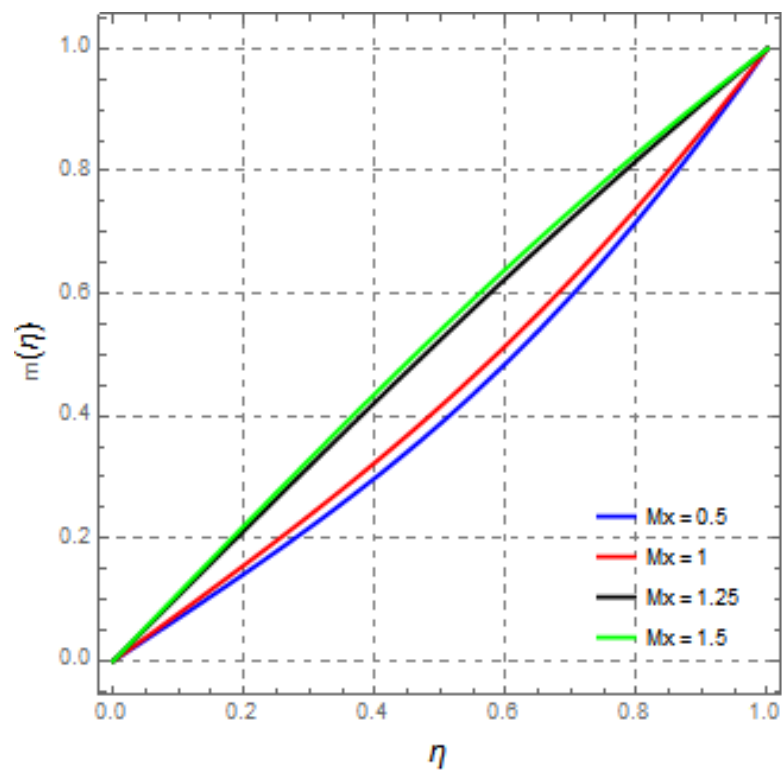


Figure 11. Impact of magnetic field strength M_x on magnetic field component m , keeping $S_z = -1.75$, $M_y = 3$, $R_m = 1$, and $S = 1$.

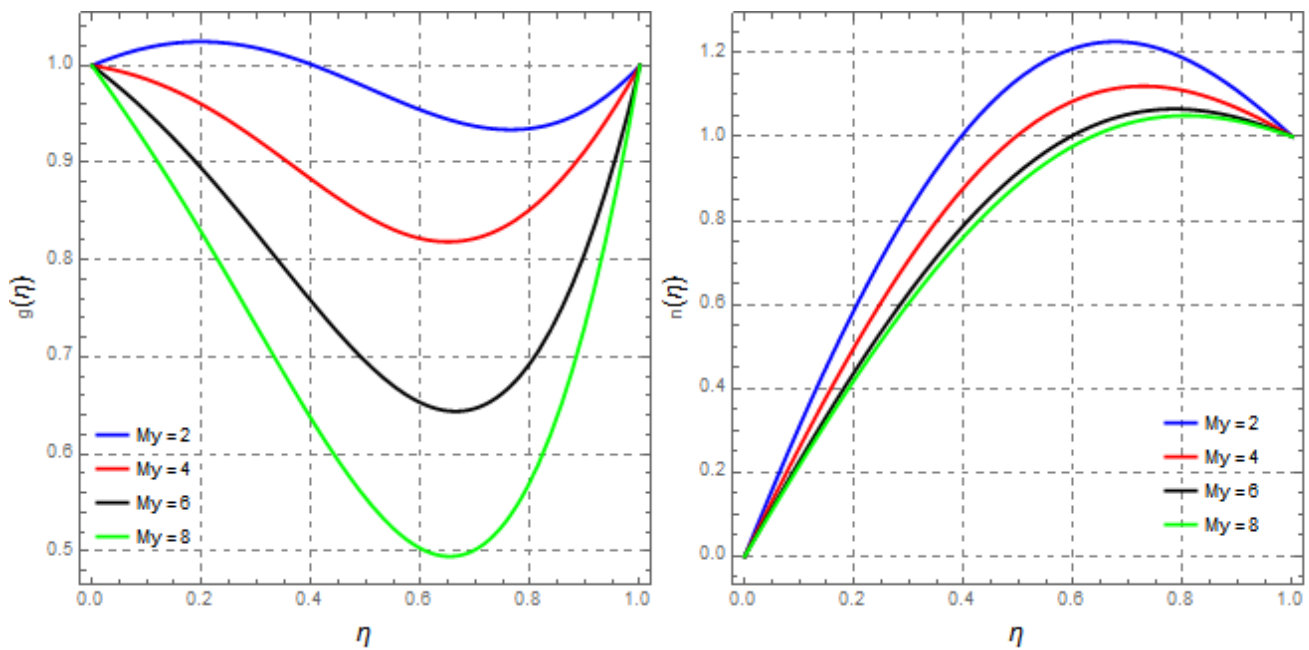


Figure 12. Impact of magnetic field strength M_y on velocity component g and magnetic field component n , keeping $S_z = -0.5$, $M_x = -0.5$ (for g), $M_x = -1.5$ (for n), $R_m = -2$ (for g), $R_m = -1$ (for n), and $S = 1$.

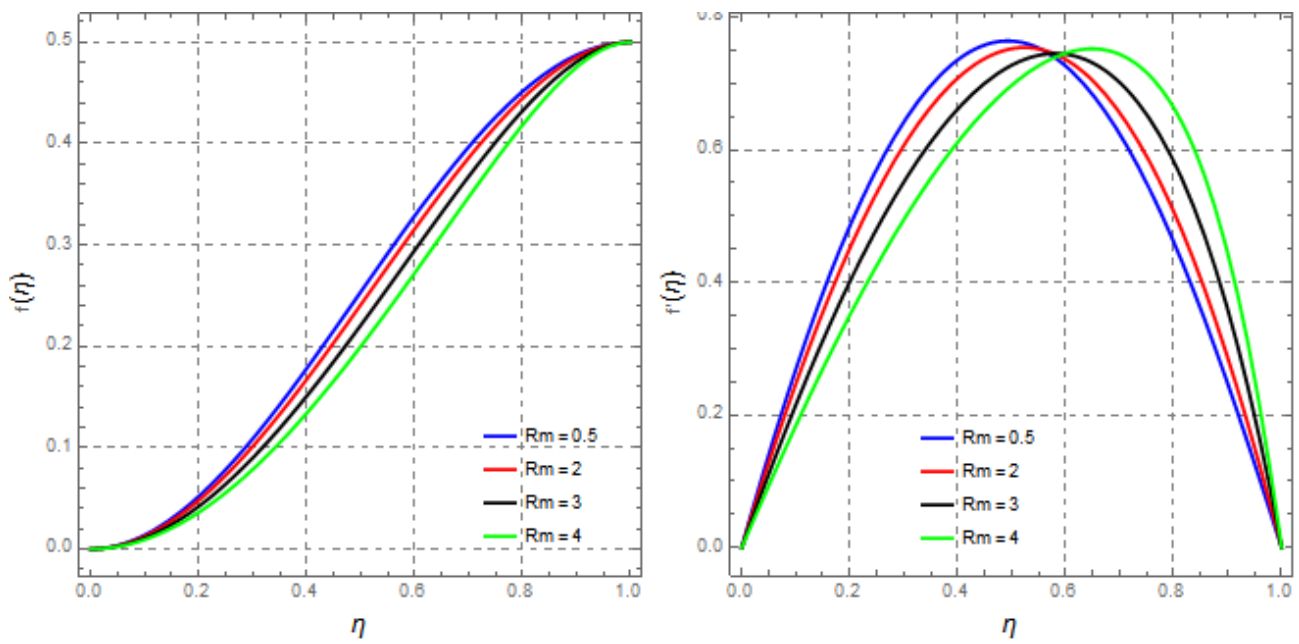


Figure 13. Impact of magnetic Reynolds number R_m on velocity component f and f' , keeping $S_z = -1.5$, $M_x = -1.5$, $M_y = 3$, and $S = 1$.

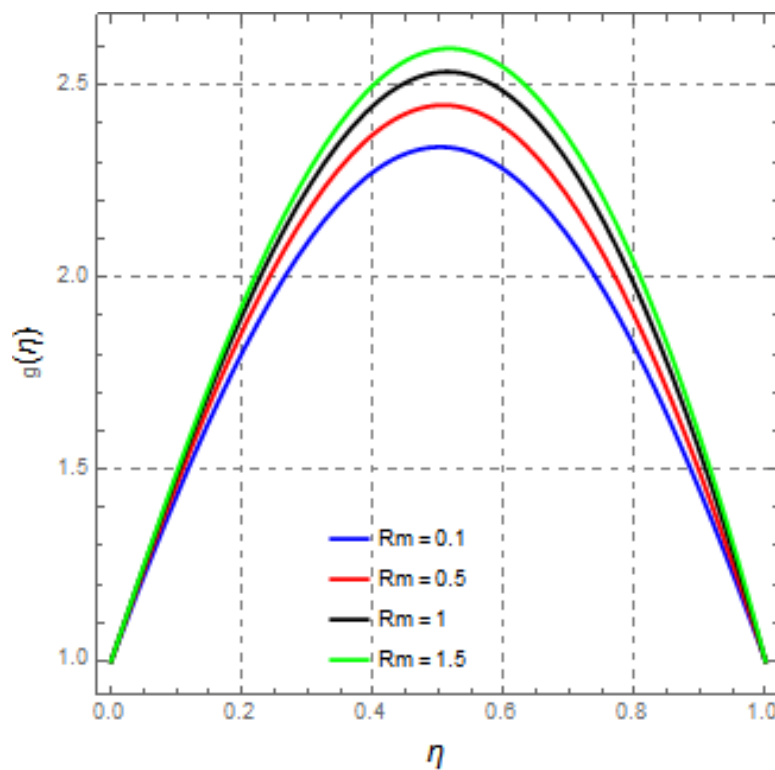


Figure 14. Impact of magnetic Reynolds number R_m on velocity component g , keeping $S_z = -1.5$, $M_x = -0.75$, $M_y = 1$, and $S = 1$.

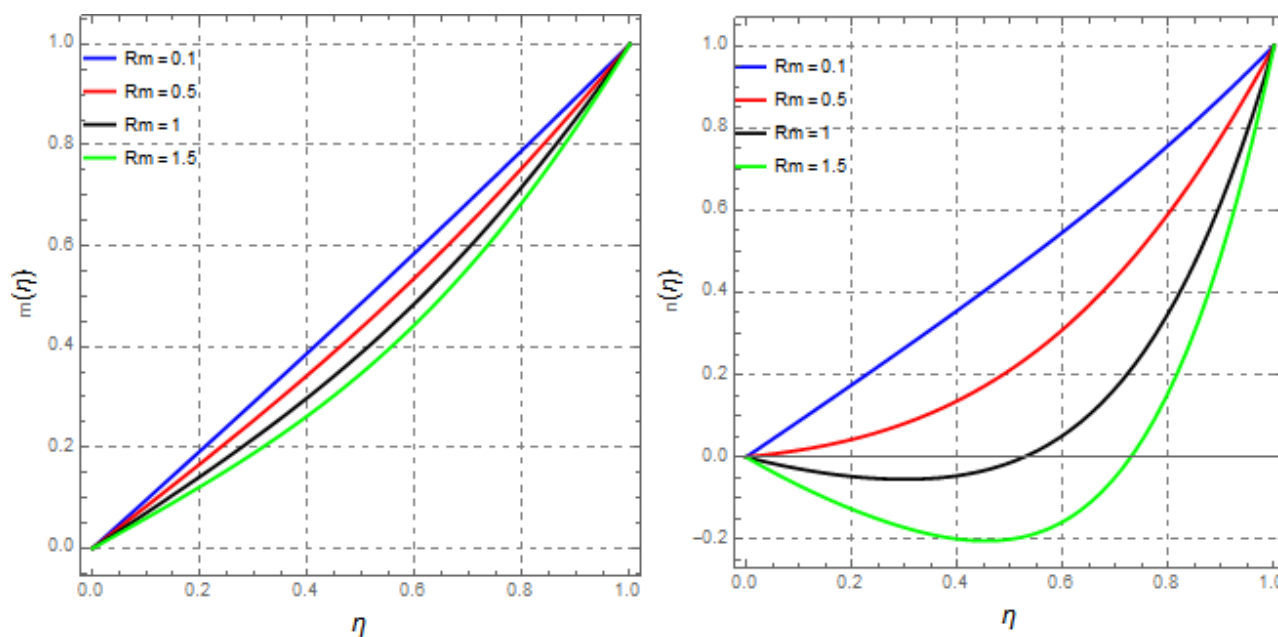


Figure 15. Impact of magnetic Reynolds number R_m on magnetic field components m and n , keeping $S_z = -1.5$, $M_x = -0.75$, $M_y = 1$, and $S = 1$.

8. Conclusions

In this paper, the 3-D squeezing MHD flow of viscous fluids was considered between two parallel plates, where both the plates are rotating with the same angular velocities. The effect of the variable magnetic field was applied and the phenomenon was modeled using the coupled governing equations, i.e., continuity, Navier–Stokes, and the magnetic field equation. Furthermore, by using the suitable similarity transformation, the modeled equations of the flow phenomena were transformed to the ordinary differential Equations (8)–(11) and were solved by using the analytical technique (HAM) using Mathematica package BVPh 2.0. The error analysis was carried out up to 10^{-40} th order, and the effect of different parameters on the velocity and magnetic field were observed through graphs and tables. Given below are some conclusions made from the above analysis:

- It was observed that increasing the squeeze effect on the upper plate causes an increase in the flow velocity along the y - and z -direction, while along the x -direction, the velocity increase initially, but a decrease in the velocity has been observed in the upper domain ($\eta \rightarrow 1$).
- It was also investigated and concluded that, by increasing the squeeze Reynolds number, the magnetic field component decreased the effect of the magnetic field along the z -component, whereas the effect increased along the y -component.
- Furthermore, from the above problem, it was observed that increasing the magnetic field strength parameter M_x , which is the strength of the magnetic field along the x -axis, increases the fluid velocity along the z -axis; however, velocity along the y -axis showed a gradual decrease by increasing M_x . Moreover, along the x -axis, first an increase in the velocity component was observed, but as $\eta \rightarrow 1$ the velocity started decreasing.
- An inverse relation was observed between the magnetic field strength parameter M_x and the magnetic field component along the z -axis, i.e., increasing the value of M_x showed a decreasing effect in the value of the magnetic field along the z -component, and a direct relation could be seen along the y -axis.
- Furthermore, it was seen that an increasing value of the magnetic field strength parameter along the y -component caused a decrease in the velocity of the fluid along the y -axis and the effect of the magnetic field along the y -axis.

- It is concluded that for the magnetic Reynolds number R_m , a decrease in the flow velocity along the z -axis was observed with increasing R_m . On the other hand, velocity along the y -axis showed an increasing effect by increasing the R_m flow velocity along the x -axis; this showed a decreasing pattern initially, but as $\eta \rightarrow 1$, an increasing effect was observed.
- It was also observed that for the magnetic field, increasing the magnetic Reynolds number showed a decrease in the value of the magnetic field along both the y - and z -axes.

Author Contributions: Conceptualization, M.K.A.; Data curation, M.K.A.; Formal analysis, M.K.A. and U.F.G.; Funding acquisition, S.N.; Investigation, K.B.; Methodology, M.K.A. and U.F.-G.; Resources, U.F.-G.; Writing—review & editing, A.K. and U.F.-G. All authors have read and agreed to the published version of the manuscript.

Funding: The work of U.F.-G. was supported by the government of the Basque Country for the ELKA-RTEK21/10 KK-2021/00014 and ELKARTEK20/78 KK-2020/00114 research programs, respectively.

Institutional Review Board Statement: Not applicable.

Informed Consent Statement: Not applicable.

Data Availability Statement: Not applicable.

Conflicts of Interest: The authors declare no conflict of interest.

References

1. Siddiqui, A.M.; Irum, S.; Ansari, A.R. Unsteady squeezing flow of a viscous MHD fluid between parallel plates, a solution using the homotopy perturbation method. *Math. Model. Anal.* **2008**, *13*, 565–576. [CrossRef]
2. Sweet, E.; Vajravelu, K.; Van Gorder, R.A.; Pop, I. Analytical solution for the unsteady MHD flow of a viscous fluid between moving parallel plates. *Commun. Nonlinear Sci. Numer. Simul.* **2011**, *16*, 266–273. [CrossRef]
3. Sri Ramachandra Murty, P.; Balaji Prakash, G. MHD Two-Fluid Flow and Heat Transfer between Two Inclined Parallel Plates in a Rotating System. *Int. Sch. Res. Not.* **2014**, *2014*, 256898. [CrossRef]
4. Onyango, E.R.; Kinyanjui, M.; Kimathi, M. Unsteady Hydromagnetic Flow between Parallel Plates Both Moving in the Presence of a Constant Pressure Gradient. 2017. Available online: http://www.ijesit.com/Volume%206/Issue%201/IJESIT201701_11.pdf (accessed on 1 March 2022).
5. Khan, M.S.; Shah, R.A.; Khan, A. Effect of variable magnetic field on the flow between two squeezing plates. *Eur. Phys. J. Plus.* **2019**, *134*, 219. [CrossRef]
6. Muhammad, T.; Hayat, T.; Alsaedi, A.; Qayyum, A. Hydromagnetic unsteady squeezing flow of Jeffrey fluid between two parallel plates. *Chin. J. Phys.* **2017**, *55*, 1511–1522. [CrossRef]
7. Verma, P.D.; Mathur, A. Magnetohydrodynamic Flow between Two Parallel Plates, One in Uniform Motion and the Other at Rest with Uniform Suction at the Stationary Plate. *Proc. Indian Natl. Sci. Acad.* **1969**, *35*, 507–517.
8. Hayat, T.; Sajjad, R.; Alsaedi, A.; Muhammad, T.; Ellahi, R. On squeezed flow of couple stress nanofluid between two parallel plates. *Results Phys.* **2017**, *7*, 553–561. [CrossRef]
9. Linga Raju, T. MHD heat transfer two-ionized fluids flow between parallel plates with Hall currents. *Results Eng.* **2019**, *4*, 100043. [CrossRef]
10. Hamza, E.A. The magnetohydrodynamic effects on a fluid film squeezed between two rotating surfaces. *J. Phys. Appl. Phys.* **1991**, *24*, 547–554. [CrossRef]
11. Das, S.; Maji, S.L.; Guria, M.; Jana, R.N. Unsteady MHD Couette flow in a rotating system. *Math. Comput. Model.* **2009**, *50*, 1211–1217. [CrossRef]
12. Parter, S.V.; Rajagopal, K.R. Swirling Flow between Rotating Plates. In *The Breadth and Depth of Continuum Mechanics*; Springer: Berlin/Heidelberg, Germany, 1986; ISBN 978-3-642-61634-1.
13. Rajagopal, K.R.; Parter, S.V. Remarks on the flow between two parallel rotating plates. *Tech. Summ. Rep. Wis. Univ.* **1984**. Available online: <https://ui.adsabs.harvard.edu/abs/1984wisc.reptQ....P/abstract> (accessed on 1 March 2022).
14. Rajagopal, K.R. The flow of a second order fluid between rotating parallel plates. *J. Non-Newton. Fluid Mech.* **1981**, *9*, 185–190. [CrossRef]
15. Tripathi, R.; Seth, G.; Manoj, M. Double diffusive flow of a hydromagnetic nanofluid in a rotating channel with Hall effect and viscous dissipation: Active and passive control of nanoparticles. *Adv. Powder Technol.* **2017**, *28*, 2630–2641. [CrossRef]
16. Hughes, W.; Elco, R. Magnetohydrodynamic lubrication flow between parallel rotating disks. *J. Fluid Mech.* **1962**, *13*, 21–32. [CrossRef]

17. Elshekh, S.S.; Abd Elhady, M.K.; Ibrahim, F.N. Fluid film squeezed between two rotating disks in the presence of a magnetic field. *Int. J. Eng. Sci.* **1996**, *34*, 1183–1195. [[CrossRef](#)]
18. Shah, R.A.; Khan, A.; Shuaib, M. On the study of flow between unsteady squeezing rotating discs with cross diffusion effects under the influence of variable magnetic field. *Heliyon* **2018**, *4*, e00925. [[CrossRef](#)]
19. Ganji, D.D.; Abbasi, M.; Rahimi, J.; Gholami, M.; Rahimipetroudi, I. On the MHD squeeze flow between two parallel disks with suction or injection via HAM and HPM. *Front. Mech. Eng.* **2014**, *9*, 270–280. [[CrossRef](#)]
20. Khan, A.; Shah, R.A.; Shuaib, M.; Ali, A. Fluid dynamics of the magnetic field dependent thermosolutal convection and viscosity between coaxial contracting discs. *Results Phys.* **2018**, *9*, 923–938. [[CrossRef](#)]
21. Munawar, S.; Mehmood, A.; Ali, A. Three-dimensional squeezing flow in a rotating channel of lower stretching porous wall. *Comput. Math. Appl.* **2012**, *64*, 1575–1586. [[CrossRef](#)]
22. Alzahrani Abdullah, K.; Zaka, U.M.; Taseer, M. Numerical Treatment for 3D Squeezed Flow in a Rotating Channel With Soret and Dufour Effects. *Front. Phys.* **2020**, *8*, 201. [[CrossRef](#)]
23. Shah, Z.; Gul, T.; Islam, S.; Khan, M.A.; Bonyah, E.; Hussain, F.; Mukhtar, S.; Ullah, M. Three dimensional third grade nanofluid flow in a rotating system between parallel plates with Brownian motion and thermophoresis effects. *Results Phys.* **2018**, *10*, 36–45. [[CrossRef](#)]
24. Riasat, S.; Ramzan, M.; Kadry, S.; Chu, Y.-M. Significance of magnetic Reynolds number in a three-dimensional squeezing Darcy-Forchheimer hydromagnetic nanofluid thin-film flow between two rotating disks. *Sci. Rep.* **2020**, *10*, 17208. [[CrossRef](#)]
25. Fiza, M.; Alsubie, A.; Ullah, H.; Hamadneh, N.N.; Islam, S.; Khan, I. Three-Dimensional Rotating Flow of MHD Jeffrey Fluid Flow between Two Parallel Plates with Impact of Hall Current. *Math. Probl. Eng.* **2021**, *2021*, 6626411. [[CrossRef](#)]
26. Kamran Alam, M.; Bibi, K.; Khan, A.; Noeiaghdam, S. Dufour and Soret Effect on Viscous Fluid Flow between Squeezing Plates under the Influence of Variable Magnetic Field. *Mathematics* **2021**, *9*, 2404. [[CrossRef](#)]
27. Waqas, H.; Farooq, U.; Ibrahim, A.; Kamran Alam, M.; Shah, Z.; Kumam, P. Numerical simulation for bioconvective flow of burger nanofluid with effects of activation energy and exponential heat source/sink over an inclined wall under the swimming microorganisms. *Sci. Rep.* **2021**, *11*, 14305. [[CrossRef](#)]
28. Khan, A.; Shah, R.A.; Kamran Alam, M.; Ahmed, H.; Shahzad, M.; Rehman, S.; Ahmed, S.; Sohail Khan, M.; Abdel-Aty, A.-H.; Zakary, M. Computational investigation of an unsteady non-Newtonian and non-isothermal fluid between coaxial contracting channels: A PCM approach. *Results Phys.* **2021**, *28*, 104570. [[CrossRef](#)]
29. Shah, Z.; Khan, A.; Alam, M.K.; Khan, W.; Islam, S.; Kumam, P.; Thounthong, P. Micropolar Gold Blood Nano fluid flow and Radioactive Heat Transfer between Permeable Channels. *Comput. Methods Programs Biomed.* **2020**, *186*, 105197. [[CrossRef](#)]
30. Burgan, H.I.; Aksoy, H. Daily flow duration curve model for ungauged intermittent subbasins of gauged rivers. *J. Hydrol.* **2022**, *604*, 127429. [[CrossRef](#)]